In vivo Photoacoustic Molecular Imaging with Simultaneous Multiple Selective Targeting Using Antibody-Conjugated Gold Nanorods

Pai-Chi Li,[1,2,*] Churng-Ren Chris Wang,[3] Dar-Bin Shieh,[4,5] Chen-Wei Wei,[2] Chao-Kang Liao,[2] Carolina Poe,[3] Suwen Jhan,[3] Ann-Ann Ding,[4] and Ya-Na Wu[4]

[1]*Graduate Institute of Biomedical Electronics and Bioinformatics, National Taiwan University, Taipei, Taiwan 106*
[2]*Department of Electrical Engineering, National Taiwan University, Taipei, Taiwan 106*
[3]*Department of Chemistry and Biochemistry, National Chung-Cheng University, Chia-Yi, Taiwan 621*
[4]*Institute of Molecular Medicine, National Cheng-Kung University, Tainan, Taiwan 701*
[5]*Institute of Oral Medicine, National Cheng-Kung University, Tainan, Taiwan 701*
[*]*Corresponding author: paichi@cc.ee.ntu.edu.tw*

Abstract: The use of gold nanorods for photoacoustic molecular imaging with simultaneous multiple targeting is reported. Multiple targeting is done by utilizing the tunable optical absorption property of gold nanorods. This technique allows multiple molecular signatures to be obtained by simply switching laser wavelength. HER2 and EGFR were chosen as the primary target molecules for examining two cancer cells, OECM1 and Cal27. Both *in vitro* and *in vivo* mouse model imaging experiments were performed, with contrast enhancement of up to 10dB and 3.5dB, respectively. The potential in improving cancer diagnosis is demonstrated.

OCIS codes: (170.5120) Photoacoustic imaging; (170.3880) Medical and biological imaging.

References and links

1. K. Shah, A. Jacobs, X. O. Breakefield, and R. Weissleder, "Molecular imaging of gene therapy for cancer," Gene Ther. **11**, 1175–1187 (2004).
2. X. Gao, Y. Cui, R. M. Levenson, L. W. K. Chung, and S. Nie, "*In vivo* cancer targeting and imaging with semiconductor quantum dots, » Nat. Biotechnol. **22**, 969–976 (2004).
3. D. B. Ellegala, H. Leong-Poi, J. E. Carpenter, A. L. Klibanov, S. Kaul, M. E. Shaffrey, J. Sklenar, and J. R. Lindner, "Imaging tumor angiogenesis with contrast ultrasound and microbubbles targeted to $\alpha_v\beta_3$," Circulation **108**, 336–341 (2003).
4. L. Josephson, M. F. Kircher, U. Mahmood, Y. Tang, and R. Weissleder, "Near-infrared fluorescent nanoparticles as combined MR/optical imaging probes," Bioconjug. Chem. **13**, 554–560 (2002).
5. S. R. Cherry, "*In vivo* molecular and genomic imaging: new challenges for imaging physics," Phys. Med. Biol. **49**, R13–R48 (2004).
6. P.-C. Li, C.-W. Wei, C.-K. Liao, C.-D. Chen, K.-C. Pao, C.-R. Chris Wang, Y.-N. Wu, and D.-B. Shieh, " Photoacoustic imaging of multiple targets using gold nanorods," IEEE Trans. Ultrason. Ferroelectr. Freq. Control **54**, 1642-1647 (2007).
7. R. O. Esenaliev, A. A. Karabutov, and A. A. Oraevsky, "Sensitivity of laser opto-acoustic imaging in detection of small deeply embedded tumors," IEEE J. Sel. Top. Quantum Electron. **5**, 981–988 (1999).
8. J. A. Viator, L. O., Svaasand, G. Aguilar, B. Choi, and J. S. Nelson, "Photoacoustic measurement of epidermal melanin," Proc. SPIE **4960**, 14–20 (2003).
9. R. O. Esenaliev, I. V. Larina, K. V. Larin, D. J. Deyo, M. Motamedi, and D. S. Prough, "Optoacoustic technique for noninvasive monitoring of blood oxygenation: a feasibility study," Appl. Opt. **41**, 4722–4731 (2002).
10. C. W. Wei, S. W. Huang, C. R. C. Wang, and P.-C. Li, "Photoacoustic flow measurements based on wash-in analysis of gold nanorods," IEEE Trans. Ultrason. Ferroelectr. Freq. Control **54**, 1131–1141 (2007).
11. D. L. Chamberland, A. Agarwal, N. Kotov, J. B. Fowlkes, P. L. Carson, and X. Wang, "Photoacoustic tomography of joints aided by an Etanercept-conjugated gold nanoparticle contrast agent—an *ex vivo* preliminary rat study, " Nanotechnology **19**, 095101 (2008).

#98198 - $15.00 USD Received 2 Jul 2008; revised 26 Oct 2008; accepted 27 Oct 2008; published 28 Oct 2008

12. J. A. Copland, M. Eghtedari, V. L. Popov, N. Kotov, N. Mamedova, M. Motamedi M, and A. A. Oraevsky, "Bioconjugated gold NPs as a molecular based contrast agent: implications for imaging of deep tumors using optoacoustic tomography," Mol. Imaging Biol. **6,** 341–9 (2004).
13. S. Link and M. A. El-Sayed, "Spectral properties and relaxation dynamics for surface plasmon electronic oscillations in gold and silver nanodots and nanorods," J. Phys. Chem. B **103**, 8410–8426 (1999).
14. F. Meric-Bernstam and M. C. Hung, "Advances in Targeting Human Epidermal Growth Factor Receptor-2 Signaling for Cancer Therapy," Clin. Cancer Res. **12**, 6326–6330 (2006).
15. S. Kalyankrishna and J. R. Grandis, "Epidermal Growth Factor Receptor Biology in Head and Neck Cancer," J. Clin. Oncol. **24**, 2666–2672 (2006).
16. Y. Y. Yu, S. S. Chang, C. L. Lee, and C. R. C. Wang, "Gold nanorods: electrochemical synthesis and optical properties," J. Phys. Chem. B **101**, 6661–6664 (1997).
17. S. S. Chang, C. W. Shih, C. D. Chen, W. C. Lai, and C. R. C. Wang, "The shape transition of gold nanorods," Langmuir **15**, 701–709 (1999).
18. C. W. Shih, W. C. Lai, C. C. Hwang, S. S. Chang, and C. R. C. Wang, *Metal Nanoparticles: Synthesis, Characterization, and Application* (Marcel Dekker, 2001), Chap. 7.
19. L. R. Hirsch, J. B. Jackson, A. Lee, N. J. Halas, and J. L. West, "A whole blood immunoassay using gold nanoshells," Anal. Chem. **75**, 2377–2381 (2003).
20. H. Liao, J. H. Hafner, "Gold nanorod bioconjugates," Chem. Mater. **17**, 4636–4641 (2005).
21. "Optical Absorption Spectra," http://omlc.ogi.edu/spectra/index.html.
22. G. F. Paciotti, L. Myer, D. G. I. Kingston, T. Ganesh, and L. Tamarkin, "Colloidal gold nanoparticles: a versatile platform for developing tumor targeted cancer therapies," NSTI-Nanotech. **1**, 7–10 (2005).

1. Introduction

Molecular imaging refers to remote sensing the characteristics of biological process and interactions at the molecular level [1]. It has a great potential for the early detection and more effective treatment of diseases, because aberrations at the cellular and molecular levels occur much earlier than anatomic changes. In general, specific targeting employs an exogenous nanoprobe that has a high affinity to the molecule (i.e., the biomarker) associated with a specific type of disease, with the targeting of probes tracked using a suitable imaging system. Molecular imaging methods have been developed for various imaging modalities. For example, X. Gau *et al*. have developed nanoprobes based on semiconductor quantum dots for cancer targeting and fluorescence imaging in living mice [2]. For ultrasound imaging, microbubbles targeted to $\alpha_v\beta_3$-integrins expressed on the endothelium cells were used for imaging angiogenesis [3]. L. Josephson *et al*. have shown that peptide-conjugated magnetic nanoparticles can target lymph modes and be used as an MR contrast agent [4]. On the other hand, S. R. Cherry mentioned that several groups have considerable success in small animal imaging by using nuclear imaging system including PET and SPECT with the use of radionuclides-labeled probes [5].

The goal of targeting cancer cells is to determine the expressions of oncogenic surface molecules, which will aid the prediction of clinical outcomes and treatment responses. For this it is necessary to image cancer lesions and obtain pathogenic information on them at the molecular level. However, most previous researches reported in the literature have employed only a single target. Therefore, the goal of this study was to realize *in vivo* photoacoustic (PA) imaging with simultaneous multiple selective targeting for cancer diagnosis. We have previously demonstrated *in vitro* multiple targeting [6], and the present study further demonstrates the *in vivo* imaging of small-animal models and extravasation of multiple molecular probes.

PA imaging is a new imaging modality under preclinical development that has been applied to several biomedical applications for obtaining anatomic and functional information, including breast tumor detection [7], epidermal melanin measurements [8], blood oxygenation monitoring [9], and quantitative blood flow estimation [10]. For molecular imaging

#98198 - $15.00 USD Received 2 Jul 2008; revised 26 Oct 2008; accepted 27 Oct 2008; published 28 Oct 2008

applications, Chamberland *et al*. have found that the intrinsic contrast of rat tail joint in photoacoutic tomography can be enhanced by administration of Etanercept-conjugated gold nanorods, which helps to monitor anti-tumor necrosis factor drug delivery [11]. Also, J. A. Copland et al. have used antibody-conjugated gold nanospheres for breast cancer cell targeting [12]. In the current study, cylindrical antibody-conjugated gold nanorods (AuNRs) were used as nanoprobes for PA imaging to achieve multiple selective targeting. The wavelength at which the optical absorption of gold nanorods is maximal increases with their aspect ratio [13], and AuNRs with different aspect ratios can be conjugated to different antibodies and detected by irradiation with laser pulses at appropriate wavelengths.

To achieve simultaneous multiple targeting, different antibodies and a blocker (PEG) are conjugated to AuNRs with different aspect ratios to form various types of nanoprobes that are injected into blood vessels at the same time. The purpose of attaching blockers is to avoid nonspecific binding such as electrostatic binding and endocytosis. The extravasating nanoprobes can target cancer cells with antigens specific to the conjugated antibody. Consequently, different types of cancer cells can be recognized and multiple characteristics can be obtained with laser irradiation at wavelengths corresponding to the peak absorption wavelengths of the nanoprobes.

This study used oral cancer OECM1 (oral squamous cell carcinoma) cells with HER2 (human epidermal growth factor receptor 2) overexpressed on the cell surface, and Cal27 (squamous cell carcinoma) cells with EGFR (epidermal growth factor receptor) overexpressed on the cell surface. These two cell types, each with a specific cell–antibody pair, were adopted to demonstrate multiple selective targeting.

HER2 expression is associated with growth characteristics and sensitivity to Herceptin chemotherapy, and is a member of the HER tyrosine kinase family that regulates cell growth and proliferation. HER2 has been associated with an aggressive phenotype and a poor prognosis, making it an appealing therapeutic target [14].

EGFR expression is strongly correlated with tumor metastasis. It is overexpressed in several epithelial malignancies, including head and neck squamous cell carcinoma (HNSCC), with 90% of such tumors exhibiting EGFR overexpression. EGFR plays a critical role in HNSCC growth, invasion, metastasis, and angiogenesis [15].

To demonstrate multiple targeting, two types of nanoprobes were prepared: $AuNR_{785}$-HER2 and $AuNR_{1000}$-EGFR; where the subscripts represent the peak absorption wavelengths of two types of gold nanorods with mean aspect ratios of 3.7 (785 nm) and 5.9 (1000 nm). Fig. 1 shows the absorption spectra of the two nanorods measured by a spectrophotometer (HP 8453, HP, Palo Alto, CA). The conjugated antibodies on the two gold nanorods were anti-HER2 and anti-EFGR, respectively. Here we first demonstrate the targeting ability of the two nanoprobes to OECM1 and Cal27. Multiple selective targeting with mixed probes (i.e., $AuNR_{785}$-HER2 and $AuNR_{1000}$-EGFR) is the focus of the on-going study.

#98198 - $15.00 USD Received 2 Jul 2008; revised 26 Oct 2008; accepted 27 Oct 2008; published 28 Oct 2008

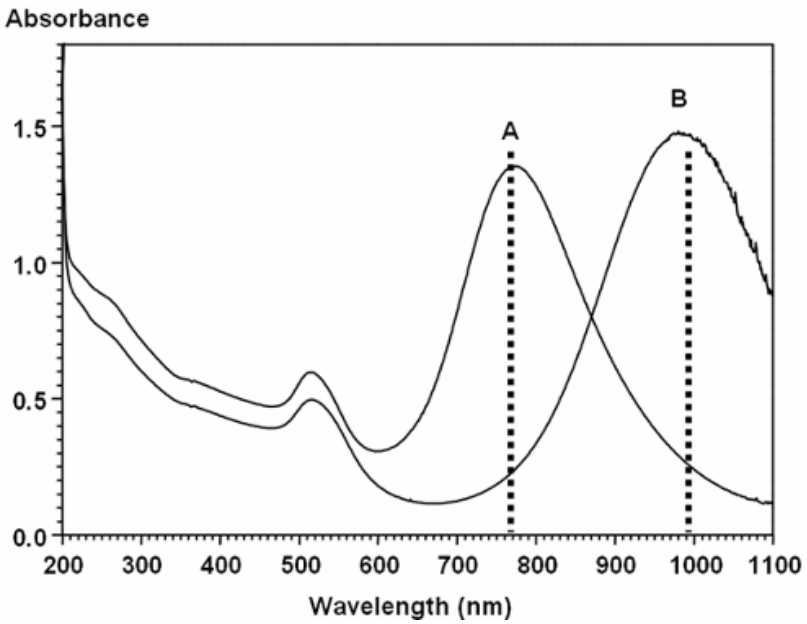

Fig. 1. Absorption spectra of gold nanorods with two aspect ratios: (A) $AuNR_{785}$ and (B) $AuNR_{1000}$.

2. Methods

In preparation of the cell culture, OECM1 cells were maintained in 90% RPMI1640 and 10% FBS (fetal bovine serum), and Cal27 cells were cultured in 90% DMEM and 10% FBS. All of the cell lines were maintained in a 37°C incubator with a humidified environment of 5% CO_2 in air.

EGFR antibody was purchased from Thermo Fisher Scientific (MA, USA). HER2 antibodies were purified from the A-HER2 hybridoma (CRL-10463) by GlycoNex (Taiwan).

Gold nanorods were synthesized by the electrochemical conversion of an anodic gold material into particles within an electrolytic cosurfactant system, which is a procedure that we have developed previously [16, 17]. The cationic surfactants used were CTABr (hexadecyltrimethylammonium bromide) and TDABr (tetradodecylammonium bromide). The particle shape was successfully controlled using cationic cosurfactant micelles that included several other ingredients such as cyclohexane and trace amount of silver ions [18]. The gold nanorods were then well dispersed in aqueous solutions. Multiple-target studies were achieved using two nanorod samples and a gold-nanosphere system exhibiting surface plasmon resonances at approximately 800 and 1000 nm for the subsequent antibody conjugation and cell binding.

In addition to successful and stable conjugation of the recognition unit to the AuNRs through chemical bonding, it was also necessary that the nanoprobes exhibited high dispersity prior to binding to cancer cells. To achieve these goals, we adopted a conjugation protocol involving a 1-ethyl-3-(3-dimethylaminopropyl) carbodiimide hydrochloride (EDC-mediated coupling reaction and subsequent attachment of a blocking agent [mPEG-SH, a thiol-terminated methoxypoly (ethyleneglycol)] at nonspecific adsorption sites on the AuNRs [19, 20].

Briefly, using HER2 as an example, the absorbance of a 1-ml aliquot of the AuNR solution was adjusted to 0.8, as measured under a 2-mm optical path length at the resonance. Five milliliters of 0.4 M cysteamine dihydrochloride and 10 ml of 16 mM HNO_3 were then added, and the solution was aged for 30 min before being centrifuged at 5500 rpm for 15 min

#98198 - $15.00 USD Received 2 Jul 2008; revised 26 Oct 2008; accepted 27 Oct 2008; published 28 Oct 2008

and redispersed into 1 ml of deionized water to remove any excess cysteamine. In a separate vial, an EDC-mediated solution was prepared by adding 0.02 g of EDC to 100 μl of aqueous 1.04 M NHS (N-hydroxysuccinimide) solution and then aging the mixture for 10 min. A 2-ml aliquot of the EDC-mediated solution was mixed with 2 ml of an 8 mg/ml solution of HER2 monoclonal antibody (mAb) in 10 mM PBS in a microcentrifugation tube and then aged for 1 hour at 4 °C. To complete the conjugation process, this modified HER2 mAb solution was then added into the previously prepared cysteamine-modified AuNR solution (1 ml) and aged for 1 hour at 4 °C. This AuNR-HER2 mAb solution was flocculated by centrifugation at 5500 rpm for 15 min and then redispersed into 1 ml of aqueous 1.04 mM mPEG-SH (MW = 5000; Nektar) solution. The dispersed solution was then aged for either 1 hour or overnight. The final solution was again centrifuged at 5500 rpm for 15 min to remove any excess mPEG-SH. The flocculates were then redispersed into a 10 mM PBS solution to produce the nanoprobes. The aqueous nanoprobe solutions remained well dispersed for at least 1 month when stored at 4 °C. The absorption spectra of the nanoprobes were measured by the spectrophotometer and showed that there was no apparent absorption peak wavelength shift from the nanorods before conjugation, thus indicating the absorption property of the nanorods does not change before/after the conjugation.

For *in vivo* studies, the cancer cells were induced on the back of NOD-scid male mice by the subcutaneous injection of 10^7 cells. The tumors were measured by the PA technique after 10–15 days of growth, and were typically 5 mm in diameter and 2–3 mm thick.

The optical irradiation was delivered by a widely tunable pulsed Ti:sapphire laser (CF-125, SOLAR TII, Minsk, Republic of Belarus) lasing 800 nm laser and an Nd:YAG laser (LS-2132 U, LOTIS TII, Minsk, Belarus) lasing 1064 nm laser, respectively. These wavelengths were chosen according to the peak absorptions of the gold nanoprobes. The pulse repetition rate was 10 Hz. A homemade PA transducer made of lithium niobate ($LiNbO_3$) material with a center frequency of 20 MHz and a focal depth of 9.5 mm was used for signal detection. The transducer had a diameter of 6 mm and a 0.65 mm hole in the center of the transducer surface for insertion of optical fiber that can solved conventional device-placing problem. Thus, the transducer can be integrated with a single fiber (FT-600-UMT, Thorlabs, Newton, NJ) with a diameter of 600 μm through the hole to achieve registered irradiation and detection. The integrated PA transducer was driven by a precision translation stage (HR8, Nanomotion, Yokneam, Israel) to perform one-dimensional cross-sectional scans of the tumor with a step size of 0.2 mm. The received acoustic waveforms were amplified by an ultrasonic receiver (5077PR, Panametrics, Waltham, MA) and then recorded at a sampling rate of 200 Msamples/second by a data acquisition card (CompuScope 14200, Gage, Lachine, QC, Canada).

Mice with tumor cells were anesthetized with halothane vapor using a vaporizer system (Fluosorber, Market Supply, UK), placed on a plate stage, and illuminated with an incandescent bulb to keep the mouse warm. Transparent ultrasonic gel (ECGEL 4000, Hometech, Taiwan) was added between the tumor region and the transducer to improve acoustic wave propagation. For mice with the OECM1 tumor, a 100-μl mixture of $AuNR_{785}$-HER2 and $AuNR_{785}$ at a concentration of 30 nM was prepared for injection, and the irradiating wavelength was 800 nm. For Cal27 tumors, a 100-μl mixture of $AuNR_{1000}$-EGFR and $AuNR_{1000}$ at a concentration of 30 nM was prepared for injection, and the irradiating wavelength was 1064 nm.

The PA experimental setup for *in vivo* imaging (Fig. 2) consisted of an optical irradiating system, a precision translation stage, a homemade animal stage, and a data acquisition card. The nanoprobes and gold nanorods (control group) were injected into the tail veins of two mice. In each mouse the targeting process was monitored at multiple time points within 24 hours after nanorod injection. At each measurement time point, the tumor was imaged in three cross sections to calculate the averaged PA intensity within the tumor region. After each PA scanning procedure, an ultrasound image was also acquired in the same region to show

#98198 - $15.00 USD Received 2 Jul 2008; revised 26 Oct 2008; accepted 27 Oct 2008; published 28 Oct 2008

anatomic information. Ultrasound images displayed on a grayscale were superimposed with the corresponding PA images displayed in red pseudocolor.

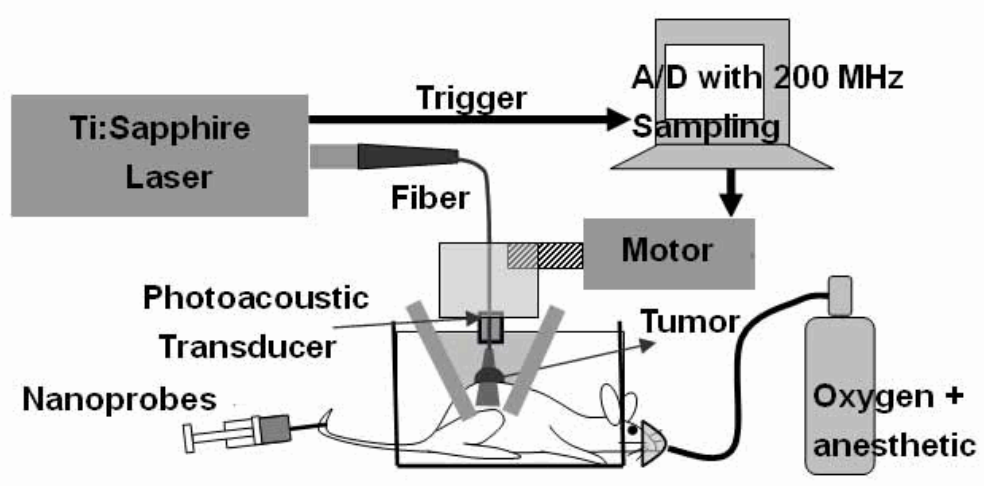

Fig. 2. Schematic diagram of the experimental setup for *in vivo* PA imaging.

3. Results

Western blot analysis can detect and indicate the size of specific proteins in a mixture. For multiple-target molecular PA imaging, the cancer cell-line bank has been screened for appropriate model cells. Fig. 3 shows that OECM1 cells overexpressed HER2 and exhibited a relatively low expression of EGFR, while Cal27 cells showed the opposite expression profile.

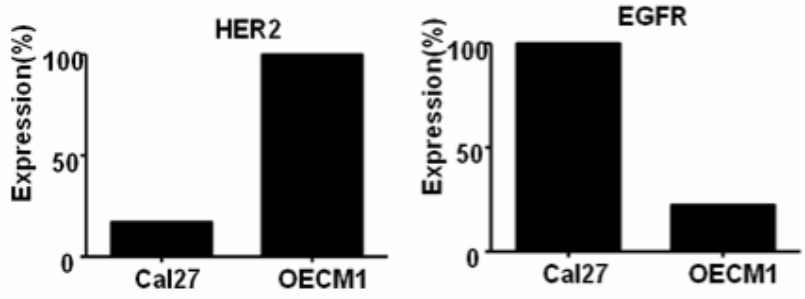

Fig. 3. Western blot analysis revealed the overexpression of HER2 in OECM1 cells and EGFR overexpression in Cal27.

Before performing *in vivo* animal experiments, *in vitro* experiments with cell cultures were performed to verify the targeting ability of the bioconjugated gold nanorods to cancer cells. The cells were collected into a centrifuge tube and adjusted the cell number to 1.2×10^6 in the ependorff tube. Then PBS containing 10% FBS (fetal bovine serum) plus probes ($AuNR_{785}$-HER2 or $AuNR_{1000}$-EGFR) or non-conjugated nanorods were added into the cells for binding reaction. The ependorff tubes were shaken in 4 °C for one hour. After the incubation, those unbinding nanorods were removed by washing in PBS and centrifuging in 2850 rpm for three times. The samples were placed in a phantom made from transparent plastic (Rexolite 1422, San Diego Plastics, CA). The phantom was 4 cm × 4 cm × 3 cm in size and contained several tubes with an internal diameter of 2.5 mm.

As shown in Fig. 4, for each cell line, the cells on the left, middle, and right in the phantom were reacted with probes of a specific targeting relation (experimental group), with

#98198 - $15.00 USD Received 2 Jul 2008; revised 26 Oct 2008; accepted 27 Oct 2008; published 28 Oct 2008

probes of a nonspecific targeting relation (control group), and with pure gold nanorods (control group).

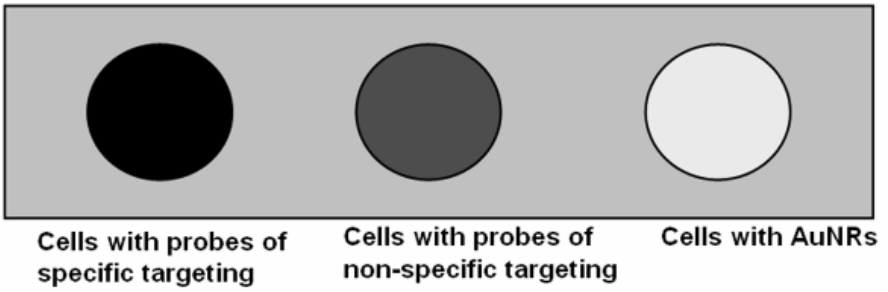

Fig. 4. Diagram of sample placement. Cells with specific targeting probes (experimental group) were in the left, cells in the control groups were in the middle, and cells with nonspecific targeting probes were in the right.

To demonstrate multiple targeting of bioconjugated gold nanorods, the two wavelengths chosen to irradiate the samples for generating PA signals (one close to and the other far from the peak absorption of the specific target probes) were 800 and 1064 nm, corresponding to the peak absorption wavelengths of the $AuNR_{785}$-HER2 and $AuNR_{1000}$-EGFR probes. The samples in the phantom were imaged in the cross-sectional view by the same PA imaging system as shown in Fig. 2 with a scan step size of 0.02 mm. The two images obtained at the two wavelengths on the same absolute scale are displayed together in Fig. 5 to compare the absolute intensities of the samples measured at different laser wavelengths. Results showed that the image intensities of the experimental groups were generally about 10 dB higher than those in the control groups. In other words, the targeting ability of specific probes to cancer cells and the wavelength selectivity of PA detection are clearly demonstrated.

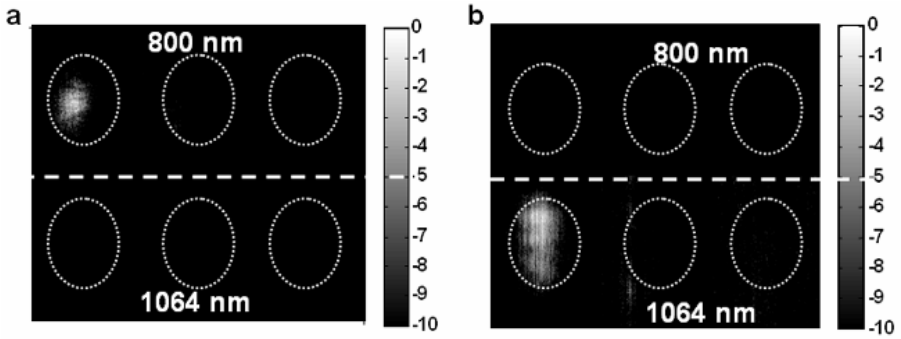

Fig. 5. (a) Images of OECM1 cells obtained at 800 and 1064 nm. OECM1 cells were with $AuNR_{785}$-HER2, $AuNR_{1000}$-EGFR, and $AuNR_{785}$ (from left to right) (b) Images of Cal27 cells obtained at 800 and 1064 nm. Cal27 cells were with $AuNR_{1000}$-EGFR, $AuNR_{785}$-HER2, and $AuNR_{1000}$ (from left to right). The images are displayed with a dynamic range of 10 dB.

The PA images of a Cal27 tumor for injections with $AuNR_{1000}$ and $AuNR_{1000}$-EGFR in Fig. 6 demonstrate the specific targeting ability of the $AuNR_{1000}$-EGFR probe. The contour of the tumor region can be clearly seen in the fusion images of PA and ultrasound images shown in Fig. 6(a) and Fig. 6(c). Also, PA images obtained at different time points post injection were shown in the same scale (25 dB dynamic range). The contrast is higher for the $AuNR_{1000}$-EGFR data postinjection (7 hours after injection) PA image within the tumor region than for the preinjection image, while there is no apparent difference between the pre- and postinjection images for the $AuNR_{1000}$ injection (Fig. 6(b) and (d)).

#98198 - $15.00 USD Received 2 Jul 2008; revised 26 Oct 2008; accepted 27 Oct 2008; published 28 Oct 2008

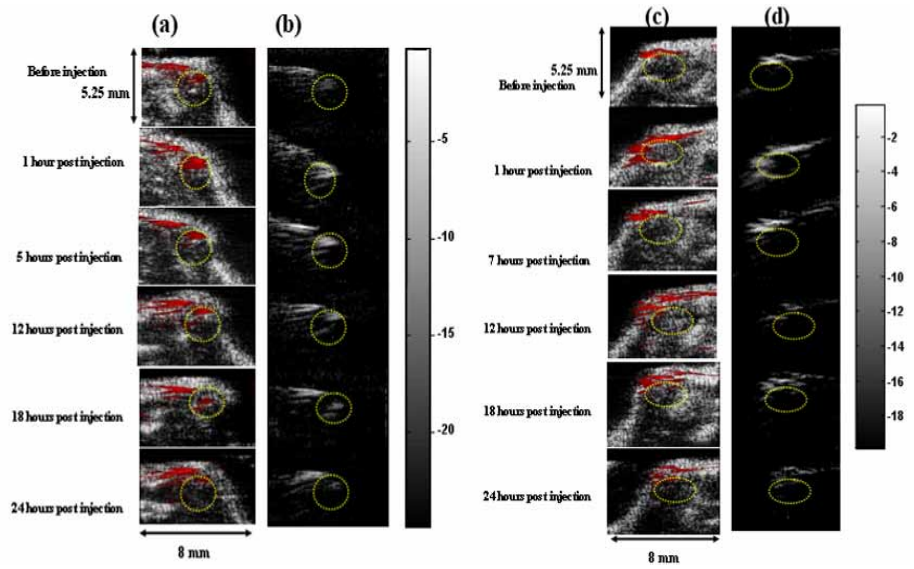

Fig. 6. Images of Cal27 tumor before and after the injection of $AuNR_{1000}$ and $AuNR_{1000}$-EGFR. Ellipses indicate the tumor regions. (a) Fusion images before/after $AuNR_{1000}$-EGFR injection at different time points. The ultrasound images are displayed on a grayscale, and the superimposed PA images obtained at an optical wavelength of 1064 nm are displayed in red pseudocolor. (b) PA images before/after $AuNR_{1000}$-EGFR injection shown in the same scale. (c) Fusion images before/after $AuNR_{1000}$ injection at different time points. The ultrasound images are displayed on a grayscale, and the superimposed PA images obtained at an optical wavelength of 1064 nm are displayed in red pseudocolor.. (d) PA images before/after $AuNR_{1000}$ injection shown in the same scale.

The PA images of OECM1 tumors in Fig. 7(a)–(d) also demonstrate the other specific cell–antibody binding relations. The postinjection images for $AuNR_{785}$-HER2 exhibited an evident increased PA intensity from 1 hour to 17 hours after injection relative to the preinjection image (Fig. 7(a), (b)). The decrease of the intensity may be due to the washout of the probes. In contrast, The pre- and postinjection images of the control group (i.e., injection of $AuNR_{785}$) showed no obvious changes in signal intensity (Fig. 7(c), (d)).

The PA signals outside of the tumor region that can be seen in Fig. 6 and Fig. 7 may be due to the signals from dermis(near the skin surface) and the fascia (with a layered appearance). The optical absorption of the dermis ranges from 2 to 10 cm^{-1} and may generate non-negligible PA signals [21]. Likewise, the fascia is between the subcutis and the muscle, the its location as shown in the histology (Fig. 8) correlates well with the PA images

#98198 - $15.00 USD Received 2 Jul 2008; revised 26 Oct 2008; accepted 27 Oct 2008; published 28 Oct 2008

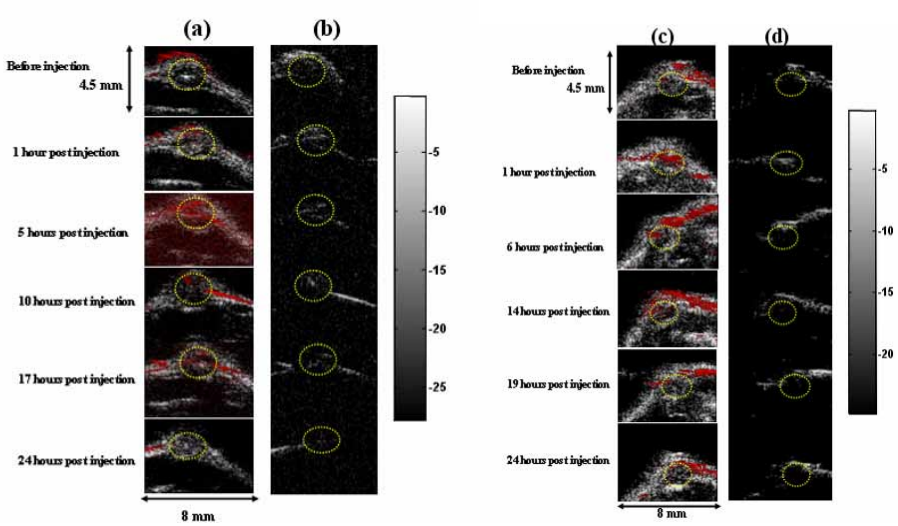

Fig. 7. Images of OECM1 tumor before and after the injection of $AuNR_{785}$ and $AuNR_{785}$-HER2. Ellipses indicate the tumor regions. (a) Fusion images before/after $AuNR_{785}$-HER2 injection at different time points. The ultrasound images are displayed on a grayscale, and the superimposed PA images obtained at an optical wavelength of 800 nm are displayed in red pseudocolor. (b) PA images before/after $AuNR_{785}$-HER2 injection shown in the same scale. (c) Fusion images before/after $AuNR_{785}$ injection at different time points. The ultrasound images are displayed on a grayscale, and the superimposed PA images obtained at an optical wavelength of 800 nm are displayed in red pseudocolor. (d) PA images before/after $AuNR_{785}$ injection shown in the same scale.

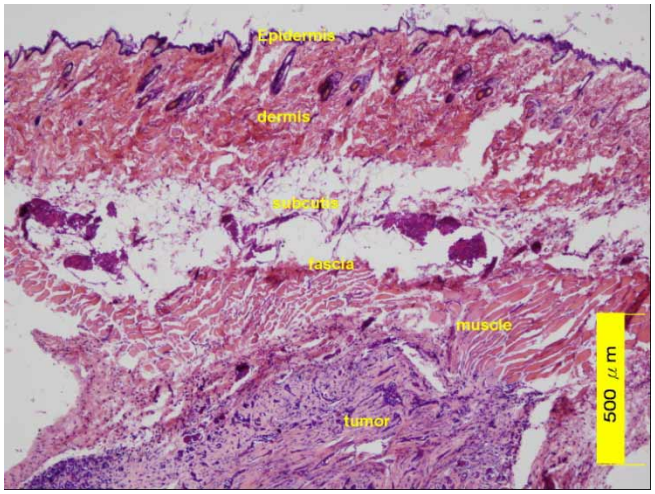

Fig. 8. Histology with a scale bar of 500 μm. Epidermis, dermis, subcutis, fascia, and muscular layers were on the top of the tumor.

The intensities of three cross-sectional PA images of the tumor region were averaged and normalized relative to the preinjection averaged intensity of the tumor region in order to quantitatively measure the targeting efficacy. As shown in Fig. 9(a), the contrast between the experimental group ($AuNR_{1000}$-EGFR injection) and the control group ($AuNR_{1000}$ injection) was maximally about 3.5 dB at 7 hours after the injection, indicating the specific targeting of $AuNR_{1000}$-EGFR to Cal27 cells. The increased intensities at 1 hour postinjection in both cases might indicate nonspecific binding due to accumulation in the circulation [22]. Fig. 9(b)

#98198 - $15.00 USD Received 2 Jul 2008; revised 26 Oct 2008; accepted 27 Oct 2008; published 28 Oct 2008

shows normalized averaged image intensities within the OECM1 tumor regions plotted as a function of the observation time. The intensity contrast between the tumor with $AuNR_{785}$-HER2 injection (solid line) and the tumor with $AuNR_{785}$ injection (dashed line) was more than 2 dB at 14 hours.

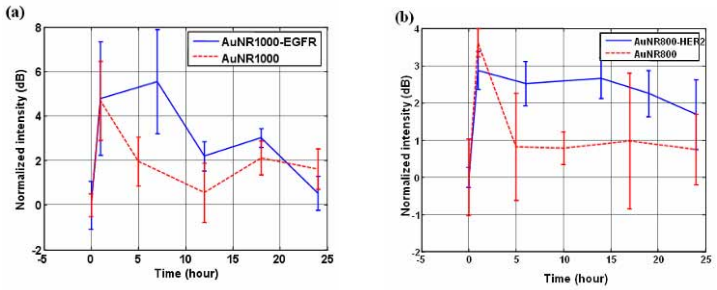

Fig. 9. (a) Averaged image intensities within the tumor region versus time after injections with $AuNR_{1000}$-EGFR (solid line) and $AuNR_{1000}$ (dashed line). (b) Averaged image intensities within the tumor region versus time after injection with $AuNR_{785}$-HER2 (solid line) and $AuNR_{785}$ (dashed line). The averages were calculated from three cross-sectional images. Error bars indicate standard deviations.

Atomic absorption (AA) spectroscopy analysis was used to confirm the targeting capability of HER2-probes. After PA imaging, the tumor tissues were surgically harvested from the mouse. The time point was 6 hours post-injection. The tumor tissues were scaled weight, homogenized, and then placed into a centrifuge tube containing 30 ml of nitric acid (12 M) for incubation for 3 days to permit complete dissolution of the tissue. The obtained liquid through was subjected to AA (UNICAM Solaar M6 series) analysis.

Figure 10 illustrates the photoacoustic images of OECM1 tumor before/after $AuNR_{785}$-HER2 injection and the averaged image intensity within the tumor regions (dashed circles). The results are consistent with Fig. 7(b) and Fig. 9(b). After probe injection, the PA intensity within tumor region increases to 3 dB higher than preinjection level. The AA spectroscopy analysis results indicate that the Au ion within tumor tissues with HER2-probe injection is 9.1 μg au^+ per gram tissue weight, while that with $AuNR_{785}$ (control group) injection is 1.23 μg au^+ per gram tissue weight.

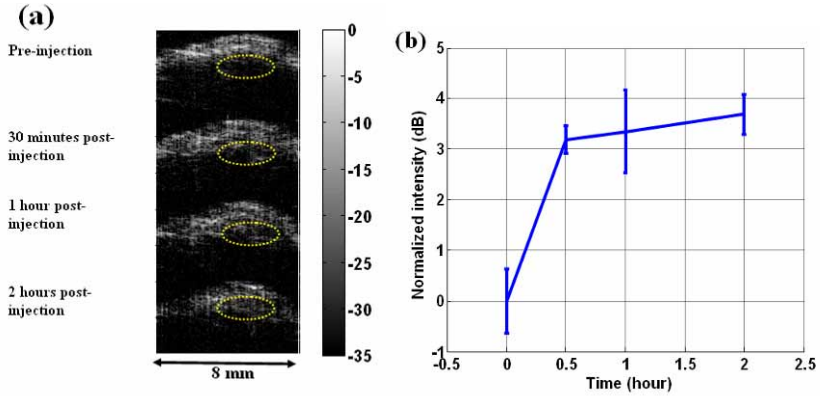

Fig. 10. (a) PA images before/after $AuNR_{785}$-HER2 injection shown in the same scale. (b) Averaged image intensities within the tumor region versus observation time.

Figure 11 illustrates the biodistribution of $AuNR_{800}$ and $AuNR_{800}$-HER2 from taken out organs after injection 24 hours by atomic absorption spectroscopy analysis. The volume for each injection was 100 μl and concentration was 5 nM. In the tumor region, the percentages of

#98198 - $15.00 USD Received 2 Jul 2008; revised 26 Oct 2008; accepted 27 Oct 2008; published 28 Oct 2008

AuNRs from the probe and $AuNR_{800}$ injection are 8.88 % and 6.1 %, respectively, thus proving the targeting capability of the probes. The results also indicate that these nanoparticles were mainly accumulated in the spleen and liver.

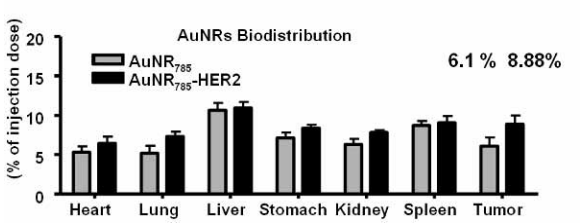

Fig. 11. Biodistribution of AuNRs of organs taken from test mice at different time period after intravenous injection of the $AuNR_{785}$ and $AuNR_{785}$-HER2. n = 3.

4. Conclusions

Utilizing the tunable optical absorption property of AuNRs, PA molecular imaging with multiple selective targeting has been demonstrated on oral cancer cells both *in vitro* and *in vivo*. The results reveal that information about multiple oncogene surface molecules of cancer cells can be obtained with PA techniques, which will help to improve our understanding of cancer cells better and to develop effective diagnosis tools as well as indications for effective treatments. This is considered as an improvement in molecular imaging compared to previous works on single targeting imaging. Note that multiple selective targeting can also be used to determine heterogeneous population of cancer cells in a lesion. Future work of this study will focus on simultaneous multiple selective targeting utilizing mixed nanoprobes (i.e., $AuNR_{785}$-HER2 and $AuNR_{1000}$-EGFR) in the same mouse. Such multiple targeting will help to recognize different cancer cells (e.g., OCEM1 and Cal27) because different cancer cells possess different expressions specific to the corresponding probes. Also, improving the contrast enhancement from the targeted AuNRs is another important task. Furthermore, a three targeting system will also be tested by adding gold nanospheres (absorption at around 520 nm) as the third molecular probe. This can be easily done because the current molecular probes have absorption peaks at around 800 nm and 1064 nm. Finally, safe and effective gold-nanoparticle-based cancer diagnoses have great potential in the pharmaceutical industry and could also make significant contributions in the biomedical field.

Acknowledgments

Financial supports from the National Science Council, the National Health Research Institutes, NTU Center for Genomic Medicine, and the NTU Nano Center for Science and Technology are gratefully acknowledged.

#98198 - $15.00 USD Received 2 Jul 2008; revised 26 Oct 2008; accepted 27 Oct 2008; published 28 Oct 2008